

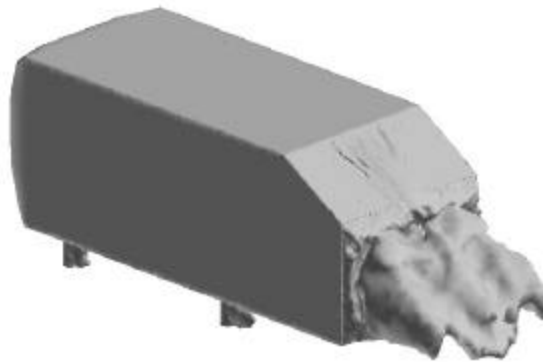


AIAA-2003-0857

Detached Eddy Simulation Over a Reference Ahmed Car Model

Sagar Kapadia and Subrata Roy
Computational Plasma Dynamics Laboratory
Kettering University, Flint, Michigan

Ken Wurtzler
Cobalt Solutions Inc.
Dayton, Ohio



41st Aerospace Sciences Meeting and Exhibit

6-9 January 2003

Reno, Nevada

Detached Eddy Simulation Over a Reference Ahmed Car Model

Sagar Kapadia* and **Subrata Roy†**
*Computational Plasma Dynamics Laboratory
Department of Mechanical Engineering
Kettering University, Flint, Michigan 48504, USA*

Ken Wurtzler‡
*Cobalt Solutions Inc.
Dayton, Ohio USA*

Turbulence modeling plays a vital role in any numerical simulation in terms of accuracy and computational cost. This paper presents a Spalart-Allmaras based detached eddy simulation hybrid model and numerical results for the Ahmed reference car model with 25° base slant angle. Highly three-dimensional and unsteady wake flow behavior is documented by showing velocity vectors in the trailing region. One-equation RANS model is also used for the same simulation. Both techniques are compared by showing the capability of each technique in capturing the minor flow details and in predicting the coefficient of drag (C_d). Finally, unsteady behavior of C_d is studied in both cases. Average value of C_d is calculated and validated with the reported experimental data of Ahmed et al. and numerical results of Gillieron and Chometon. Further, brief discussion about the present day available turbulence modeling techniques including DNS, LES, RANS and DES is also done in this paper.

INTRODUCTION

Advanced developments in automobile industry have increased the demand for the detailed three-dimensional flow analysis over a ground vehicle. The major reason of this study is to reduce the aerodynamic drag and to improve the fuel economy. Such a study can be carried out for different reference models. For example, an analysis of 3-D separated flow in automobile aerodynamics has been carried out recently.¹

Present work uses Ahmed model for the purpose of numerical simulation of the external flow analysis and drag calculation. Ahmed reference model is a car type bluff body. Ahmed model has been selected in this study due to its geometric simplicity and availability of the experimental results.^{2,3} Flow field in the wake region is considered to be complex due to the presence of three-dimensional turbulent boundary layer and heavy recirculation that consists of longitudinal, contra-rotating vortices.

Pressure drag in the wake region is the major component of total drag acting on the vehicle. Further, wake flow structure and thus pressure drag is directly dependent on the rear slant angle, indicated by α , in figure 1. Detailed study on the dependence of rear slant angle on coefficient of drag has been performed both experimentally² and numerically.⁴ A numerical study with 25° slant angle (α) has been described in the present study. Following figure shows basic dimensions and rear slant angle of the Ahmed reference model.

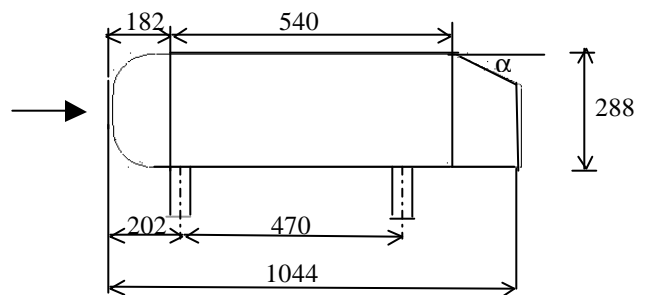


Figure 1. Ahmed reference model; dimensions are in mm.

* Graduate Research Assistant, Email: kapa9202@kettering.edu, AIAA Student member.

† Assistant Professor, Email: sroy@kettering.edu, AIAA Associate Fellow

‡ Research Engineer, Email: wurtzler@cobaltcf.com, AIAA Member

Numerical simulation is considered as one of the fastest developing branch in predicting the complex flowfield, created in the wake region of a vehicle. Experimental results give good understanding of the flow behavior as well benchmark the results to validate the numerical model used for the flow simulation. A number of numerical schemes^{4,11,12} have been developed and used for both compressible and incompressible flow analysis around a bluff body using either finite-difference or finite-volume methods. Present study uses Cobalt^{5,6}, a parallel, implicit, unstructured Euler/Navier-Stokes flow solver to produce numerical results around the Ahmed model. This code has proved very useful for high speed, massively separated flows that is common in aerospace engineering. James et al has simulated the massively separated flow around an F-15E at 65° angle of attack.⁷

One of the most important features of any CFD code is the turbulence model used by the code to predict the unsteady turbulent behavior of the flow. There are different turbulence models used in different numerical schemes.⁸ Cobalt uses several turbulence models including detached eddy simulation (DES), which is a novel feature of the present scheme. DES is a hybrid LES-RANS model and for the first time, it is used for ground vehicle flow analysis in this paper, which explores the possibility of using Cobalt and DES as a commercial software and turbulence scheme respectively in automobile industries. Spalart-Allmaras based DES model is used in the described simulation.⁹ Further, present work compares the different turbulence models in terms of accuracy and computational cost. In particular, solutions of Ahmed problem obtained by using RANS and DES turbulence models are compared. Same comparison has been done by Morton et al.¹⁰ for delta wing vortical flows using Cobalt.

Ahmed et al.² and Morel³ were the first to perform 3-D external flow analysis on Ahmed reference model. Both of these works were based on the experimental study. The primary aim of this study was to analyze the change in the drag coefficient with different rear slant angles. Ahmed et al concluded that pressure drag is the dominant component (85%) of the total drag acting on the car body and rest of the drag is the friction drag. Major part of the pressure drag is generated at the rear end (91%) and frontal part is responsible for the rest of the drag. Further, pressure drag generated at the rear end depends on rear slant angle. Critical angle (of rear slant edge) is found out to be 30°, above which, there is a sudden drop in the drag coefficient. Wake flow behavior is also directly related with the rear slant angle. At angles near to the critical angle, there are strong contra-rotating vortices and flow separates from the sloping surface and re-attaches at the bottom end of the sloping surface. For angles above the critical angle, contra-rotating vortices are found to be less

strong. Ahmed et al.² also shows the wake flow pattern for the angles near to critical angle is highly unsteady and unstable.

Several numerical simulations have been performed on Ahmed reference model.^{4,11,12} Gillieron and Chometon⁴ performed numerical simulation using k-ε model of version 4.2 of the Fluent software and compared the numerical result of drag coefficient with the experimental results obtained by Ahmed et al.² They also described the wake flow behavior for the angles, (i) between Zero and Lower critical angle, (ii) between Lower critical angle and Upper critical angle and (iii) above Upper critical angle. Flow shows 2-D behavior for first and third case, while it shows complex 3-D behavior for the second case.

Howard and Pourquie¹² have performed Large Eddy Simulation (LES) of an Ahmed reference model. Simulation has been performed for the case of 28° base slant angle, which is very near to the critical angle given by Ahmed et al.² This simulation has shown the time dependence of the drag coefficient and the flow behavior around the body.

Nomenclature:

u	X-component of the velocity
v	Y-component of the velocity
w	Z-component of the velocity
ρ	Density
p	Pressure
k	Thermal conductivity
T	Temperature
Q	Primary variable vector
Re	Reynolds Number
ν_T	Turbulence viscosity
\tilde{S}	Production term
S	Value of vorticity
C_{des}	Turbulence constant for S-A based DES model
d_w	Distance to the nearest wall
θ	Implicitness
F_d	Drag force
C_d	Total drag co-efficient
u_∞	Free stream velocity
C_{df}	Drag co-efficient in the front part
C_{db}	Drag co-efficient in the back part
f, g, h	Flux vectors
r, s, t	Viscous stress vectors
$t_{xx}, t_{xy}, t_{xz}, t_{yy}, t_{yz}, t_{zz}$	Viscous stress tensor
	Components
$\Delta x, \Delta y, \Delta z$	Mesh size in X, Y and Z direction respectively

GOVERNING EQUATIONS

Cobalt^{5,6,19,20} is used as the numerical code for the simulation presented in this paper. It solves the Euler and Navier-Stokes equations. Semi-coupled Navier-Stokes equations have been used in the present work. Following are the governing Navier-Stokes equations, written in the integral form.

$$\begin{aligned} & \frac{\partial}{\partial t} \iiint_v Q dV + \iint_d (f \hat{i} + g \hat{j} + h \hat{k}) \cdot \hat{n} dd \\ & = \iint_d (r \hat{i} + s \hat{j} + t \hat{k}) \cdot \hat{n} dd \end{aligned} \quad (1)$$

where,

$$Q = \begin{bmatrix} \mathbf{r} \\ \mathbf{ru} \\ \mathbf{rv} \\ \mathbf{rw} \\ \mathbf{re} \end{bmatrix} \quad f = \begin{bmatrix} \mathbf{ru} \\ \mathbf{ru}^2 + p \\ \mathbf{ruv} \\ \mathbf{ruw} \\ u(\mathbf{re} + p) \end{bmatrix}$$

$$g = \begin{bmatrix} \mathbf{rv} \\ \mathbf{ruv} \\ \mathbf{rv}^2 + p \\ \mathbf{rvw} \\ v(\mathbf{re} + p) \end{bmatrix} \quad h = \begin{bmatrix} \mathbf{rw} \\ \mathbf{ruw} \\ \mathbf{rvw} \\ \mathbf{rw}^2 + p \\ w(\mathbf{re} + p) \end{bmatrix}$$

$$r = \begin{bmatrix} 0 \\ \mathbf{t}_{xx} \\ \mathbf{t}_{xy} \\ \mathbf{t}_{xz} \\ a \end{bmatrix} \quad s = \begin{bmatrix} 0 \\ \mathbf{t}_{xy} \\ \mathbf{t}_{yy} \\ \mathbf{t}_{yz} \\ b \end{bmatrix} \quad t = \begin{bmatrix} 0 \\ \mathbf{t}_{xz} \\ \mathbf{t}_{yz} \\ \mathbf{t}_{zz} \\ c \end{bmatrix}$$

$$a = u\mathbf{t}_{xx} + v\mathbf{t}_{xy} + w\mathbf{t}_{xz} + k\partial T / \partial x,$$

$$b = u\mathbf{t}_{xy} + v\mathbf{t}_{yy} + w\mathbf{t}_{yz} + k\partial T / \partial y,$$

$$c = u\mathbf{t}_{xz} + v\mathbf{t}_{yz} + w\mathbf{t}_{zz} + k\partial T / \partial z.$$

\mathbf{n} - fluid element volume,

d - fluid element surface area,

\hat{n} -outward-pointing unit normal to element surface area,

$\hat{i}, \hat{j}, \hat{k}$ - Cartesian unit vectors in x, y and z direction respectively.

The ideal gas law closes the system of equations and the entire equation set is nondimensionalized by freestream density and speed of sound.

TURBULENCE MODELING

It is well known¹⁴, that the Navier-Stokes equations can describe the unsteady, turbulent flows in the continuum regime. Complex, unsteady turbulent flows can be described by using various approximations and thus, by various turbulence models.^{8,14,15} The two competing factors which are important for any turbulence model is accuracy and efficiency (i.e. computational cost). An optimal combination of both these factors are hard to achieve and thus, the primary purpose of the numerical simulation is towards attaining such a goal. The complex dynamic nature of the wake region vortices makes it necessary to model the vortices using temporally and spatially accurate calculation of the flow field using direct numerical simulation (DNS) or large eddy simulation (LES) of turbulence. A brief discussion on available turbulence modeling techniques in terms of accuracy and computational cost is presented in this section.

Of all the available turbulence models, DNS (Direct Numerical Simulation) is considered as one of the most accurate turbulent model. However, DNS explicitly accounts for all scales of motion in a turbulent flow, from the largest, imposed by the existence of boundaries or periodicities, to the smallest. The latter may be for instance the viscous thickness ν/v^* in a turbulent boundary layer, or the Kolmogorov dissipative scale $(\epsilon V^3)^{1/4}$ in three-dimensional isotropic turbulence. Kim et al. (1987) showed from that DNS of fully developed incompressible channel flow at a Reynolds number of about 6000 (based on channel height) requires grid with 2 and 4 million points. Wilcox (1993) gave the following equation to estimate the number of grid points for channel flow.

$$N_{DNS} = (0.088Re_h)^{9/4} \quad (2)$$

where Re_h is the Reynolds number based on the mean channel velocity and channel height.

This imposes critical limitation on the applicability of DNS in high Reynolds number flows. By combining above equation with the available computational resources, one can conclude that it is impossible to apply DNS for complex 3-D turbulent flows using present day computers. Contrarily, in LES the large-scale motions in the flow

Large Eddy Simulation (LES) is another growing technique to resolve unsteady turbulent flows.^{8,12} In LES, large-scale structure of turbulent flow is computed directly and the smallest and nearly isotropic eddies are modeled and can be termed as sub-grid scale eddies. This can be achieved by filtering the Navier-Stokes equations to obtain a set of equations that govern the resolved flow. Filtering is a type of space averaging of the flow variables over

regions approximately the size of the computational control volume. Computational requirements for LES is approximately (1/10) th times of that of DNS. In spite of huge computational requirement, LES is being used now days for practical problems including Ahmed Reference Model.¹²

Reynolds Average Navier-Stokes (RANS) is considered as the most practical turbulence handling technique with the present day available computational resources. The Reynolds equations are derived by decomposing the dependent variables of Navier-Stokes conservation equations into time-mean and fluctuating components and then time averaging the entire equation. As equations are averaged in this technique, additional assumptions are required to close the system of equations, which forms the base of RANS. This technique can be further classified and the most common classification is based on the number of supplementary partial differential equations that must be solved in order to supply the modeling parameters. Gillieron and Chometon⁴ used k-ε turbulence model, two-equation RANS model, for the flow analysis and drag calculation around Ahmed reference model.

As described in the previous section, each turbulence model has its own benefits and drawbacks. But if one can combine the positive features of two or more models together to construct a single model, it would have more control in terms of both accuracy and computational cost. The same philosophy has been used in Detached Eddy Simulation (DES). DES was proposed by Spalart et al.¹⁸ DES is a hybrid RANS-LES model which means it combines RANS and LES to act as a single model. Two different DES models^{9,16} are currently available in Cobalt:

- (1) S-A (Spalart-Allmaras) based DES model,
- (2) M-SST (Menter's shear stress transport) based DES model.

Spalart-Allmaras based DES model is used in the present study. S-A model and S-A based DES formulations are discussed in following two sections.

Spalart-Allmaras (S-A) model:

Spalart-Allmaras is a one equation RANS model¹⁷, which is used by Cobalt. Two simulations have been presented in this paper, one by using pure S-A turbulence model and the other by using S-A based DES model.

The S-A model solves a single partial differential equation for a variable \tilde{n} which is related to the turbulent viscosity. A transport equation for the turbulent viscosity is assembled, using empiricism and arguments of dimensional analysis, Galilean invariance and selected dependence on molecular viscosity.¹⁷

The Spalart-Allmaras turbulent kinematic viscosity is given by

$$\mathbf{n}_T = \tilde{n} f_{v1} \quad (3)$$

Following transport equation is used to calculate working variable \tilde{n} .

$$\frac{D\tilde{n}}{Dt} = c_{b1}[1 - f_{t2}]\tilde{S}\tilde{n} - \left[c_{w1}f_w - \frac{c_{b1}}{\mathbf{k}^2}f_{t2} \right] \left[\frac{\tilde{n}}{d} \right]^2 + \frac{1}{S} \left[\nabla \cdot ((\mathbf{n} + \tilde{n})\nabla\tilde{n}) + c_{b2}(\nabla\tilde{n})^2 \right] + f_{t1}\Delta U^2 \quad (4)$$

Eddy viscosity can be found out by using (3) and (4). The S-A model includes a wall destruction term to reduce the turbulent viscosity in the log layer and laminar sublayer. Trip terms are also provided in the model for smooth transition between laminar and turbulent flow. Constants and functions appear in (3) and (4) can be defined as following:

$$f_{v1} = \frac{\mathbf{c}^3}{\mathbf{c}^3 + c_{v1}^3}, \quad \mathbf{c} \equiv \frac{\tilde{n}}{\mathbf{n}} \quad (5)$$

\tilde{S} is a production term and can be express as,

$$\tilde{S} = f_{v3}S + \frac{\tilde{n}}{\mathbf{k}^2 d^2} f_{v2}, \quad (6)$$

where S is the magnitude of the vorticity and

$$f_{v2} = \left[1 + \frac{\mathbf{c}}{c_{v2}} \right]^{-3}, \quad (7)$$

$$f_{v3} = \frac{(1 + \mathbf{c}f_{v1})(1 - f_{v2})}{\mathbf{c}}, \quad (8)$$

From (6), (7) and (8), it can be seen that production term is different from that developed by Spalart and Allmaras¹⁷ due to the different formula of f_{v2} and new term f_{v3} .

Now,

$$f_w = g \left[\frac{1 + c_{w3}^6}{g^6 + c_{w3}^6} \right]^{1/6}, \quad (9)$$

$$g = r + c_{w2}(r^6 - \eta), \quad r \equiv \frac{\tilde{n}}{\tilde{S}\mathbf{k}^2 d^2}. \quad (10)$$

Trip term f_{t1} is defined as,

$$f_{i1} = c_{i1} g_i \exp\left(-c_{i2} \frac{w_i^2}{\Delta U^2} [d^2 + g_i^2 d_i^2]\right) \quad (11)$$

where, d_i is the distance from the field point to the trip, ω_i is the wall vorticity at the trip and ΔU is the difference between the velocity at the field point and that at the trip.

$g_i = \min(0.1, \Delta U / w_i \Delta x)$, where Δx is the grid spacing along the wall at the trip.

The function f_{i2} is defined as,

$$f_{i2} = c_{i3} \exp(-c_{i4} \mathbf{c}^2). \quad (12)$$

Following constants are used in equation (3) to (12).

$$c_{b1} = 0.1355, c_{b2} = 0.622, \mathbf{s} = 2/3, \mathbf{k} = 0.41,$$

$$c_{w1} = \frac{c_{b1}}{\mathbf{k}^2} + \frac{1 + c_{b2}}{\mathbf{s}}, c_{w2} = 0.3, c_{w3} = 2,$$

$$c_{v1} = 7.1, c_{v2} = 5, c_{i1} = 1, c_{i2} = 2, c_{i3} = 1.1, c_{i4} = 2.$$

Trip terms are not used in the simulation presented in this paper. Thus, transport equation (4) takes the following form for the case presented in this paper.

$$\begin{aligned} \frac{D\tilde{\mathbf{n}}}{Dt} &= c_{b1} S\tilde{\mathbf{n}} - c_{w1} f_w \left[\frac{\tilde{\mathbf{n}}}{d} \right]^2 \\ &+ \frac{1}{\mathbf{s}} \left[\nabla \cdot ((\mathbf{n} + \tilde{\mathbf{n}}) \nabla \tilde{\mathbf{n}}) + c_{b2} (\nabla \tilde{\mathbf{n}})^2 \right] \end{aligned} \quad (13)$$

Detached Eddy Simulation:

Present definition of DES¹⁶ is not linked with any specific turbulence model. According to this definition, DES is a three-dimensional unsteady numerical solution using a single turbulence model, which functions as a subgrid-scale model in regions where grid density is fine enough for an LES, and as a RANS model in regions where it is not. Spalart-Allmaras based DES model has been developed in such a way that the model works as SA RANS model near the wall surfaces and acts as a subgrid LES model away from the wall. RANS is considered as an adequate and reliable technique to predict the flow in thin shear layers and the power of LES has already shown its power to predict the flow in large separated zones. Further, progress of unsteady RANS (URANS) in achieving accuracy is not much encouraging. Thus, DES combines LES and RANS in such a way that RANS technique can be used for the flow in thin shear layers and LES can be used for large separated zones for resolution of geometry-dependent and three-dimensional eddies.

In SA based DES formulation, distance to the nearest wall, d_w is replaced by \tilde{d} , where \tilde{d} is defined as,

$$\tilde{d} = \min(d_w, C_{DES} \Delta) \quad (14)$$

where, C_{DES} is a model constant and for SA based DES model, $C_{DES} = 0.65$ and Δ is the largest distance between the cell center under consideration and the cell center of the neighbors. The definition of the neighboring cells is given in the Algorithm section of the paper.

$$\Delta = \max(\Delta x, \Delta y, \Delta z). \quad (15)$$

Equation (14) and (15) keeps the DES model in RANS SA model inside the whole attached boundary layer as streamwise or spanwise or both grid spacing parallel to the wall are at least on the order of the boundary layer thickness and thus, in (14), $\tilde{d} = d_w$ and model works as a standard SA turbulence model inside the boundary layer and the prediction of the boundary layer separation is also made by RANS mode of DES. In the regions, far from the wall, where $d_w > C_{DES} \Delta$, the length scale of the model becomes grid-dependent. The model performs as a subgrid-scale version of the S-A model for eddy viscosity. When production and destruction terms balance each other, this model reduces to an algebraic mixing-length Smagorinski-like subgrid model.

NUMERICAL ALGORITHM

Godunov's first-order accurate, exact Riemann method [13] is the foundation of the Cobalt. Cobalt is capable of achieving second-order spatial and temporal accuracies. It can handle CFL upto one million. Implicit time stepping, viscous terms and turbulence models are added in the numerical model of the Cobalt. The cell-centered, finite-volume approach is used in Cobalt due to its compactness. Arbitrary cell types in two or three dimensions may be used, and a single grid may be composed of a variety of cell types. Source terms are included to model axisymmetric cases with two-dimensional grids. The grid can be divided into groups of cells, or zones, for parallel processing. The zones needn't be physically contiguous, but usually are for efficient processing.

Figure 2 gives the clear idea of the definition of face, cell, nearest neighbor cells, next nearest-neighbor cells and the relationship between them used by Cobalt. Any face is the intersection of two opposing cells. ' J ' is the face in figure 2 and for any face ' J ', cell ' i ' indicates the left cell and ' j ' indicates the right cell. $\hat{\mathbf{n}}^J$ is the unit vector of the face J and points out of the left cell. The set of nearest-neighbor cells of a cell is defined to be those cells sharing a face

with the given cell. The set of next-nearest neighbor cells for any cell include nearest-neighbors of all nearest-neighbors, excluding the given cell itself. From this definition, one can see one to one correspondence between the faces bounding a cell and nearest-neighbor cells and thus, can be indicated with same superscript or subscript. Thus, face indices are upper case while cell indices are lower-case in Figure 2. N_i is the number of nearest-neighbor cells of cell i .

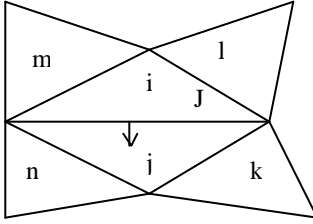


Figure 2. Definition of nearest-neighbor and next nearest-neighbor cells in Cobalt.

Five fundamental tasks comprise the flow solution algorithm: Construction of initial conditions for the Riemann problem at any given face, solution of this Riemann problem, construction of viscous fluxes at any given face, time integration and boundary conditions. The first step, constructing the initial conditions for the Riemann problem, is critical to the algorithm, for it includes any limiting or dissipation and it largely determines the spatial accuracy and truncation error of the scheme.

Discretization:

Cobalt can run both first order accurate and second order accurate cases, depends on user's choice. For the first order accuracy, constant data distribution is assumed in each cell. For the second order accuracy, data distribution is assumed to be linear in each cell. Equation used to find out the left initial state of face J for Riemann problem with second order spatial accuracy is as following:

$$q_i^J = q_i + \vec{r}_i^J \cdot \vec{\nabla} q_i \quad (16)$$

where, $q = [r, u, v, w, P]^T$ is a vector of primary variables. ' J ' and ' i ' denotes the face and cell respectively as described in the previous section. q_i^J is the estimated value at the centroid of face J due to cell i , $\vec{\nabla} q_i$ is the gradient vector and \vec{r}_i^J is a vector from the centroid of the cell i and pointing towards the centroid of face J . The gradient vector for cell i is found by a least-squares solution to (16). Right initial state for face J can be found in the similar way.

Final equation in the matrix form after considering the nearest-neighbor cells is as following:

$$A \vec{\nabla}^c q_i = \{q_m - q_i\} \quad (17)$$

$\vec{\nabla}^c q_i$ is a central difference gradient and A is an over-determined matrix due to more number of nearest-neighbor cells (equations) than unknowns. Eq(17) is solved by QR factorization.

Second order time accuracy is achieved in Cobalt and user has the facility to choose between first and second order temporal accuracy. Following equation shows the temporal integration used in Cobalt:

$$q \left\{ \mathbf{n} \frac{dQ}{dt} + \vec{\nabla} \cdot \vec{f} \right\}_i^{n+1} + (1-q) \left\{ \mathbf{n} \frac{dQ}{dt} + \vec{\nabla} \cdot \vec{f} \right\}_i^n = 0 \quad (19)$$

θ is the implicitness in the above equation. Time integration scheme can be fully explicit for $\theta=0$ and it can be fully implicit for $\theta=1$. \vec{f} is a flux vector. n and $(n+1)$ shows successive time-steps.

Temporal derivatives in the discrete form for n^{th} and $(n+1)^{\text{th}}$ time-step are as following:

$$\left(\frac{\partial Q}{\partial t} \right)^{n+1} = \frac{\mathbf{a}_{1,1}(Q^{n+1} - Q^n) + \mathbf{a}_{1,2}(Q^n - Q^{n-1})}{\Delta t} \quad (20)$$

$$\left(\frac{\partial Q}{\partial t} \right)^n = \frac{\mathbf{a}_{2,1}(Q^{n+1} - Q^n) + \mathbf{a}_{2,2}(Q^n - Q^{n-1})}{\Delta t} \quad (21)$$

For the first order temporal accuracy, $\alpha_{1,1} = \alpha_{2,1} = 1$ and $\alpha_{1,2} = \alpha_{2,2} = 0$. For the second order accuracy, $\alpha_{1,1} = 3/2$, $\alpha_{1,2} = (-1/2)$, $\alpha_{2,1} = \alpha_{2,2} = 1/2$.

The semi-discrete form of the equation used by Cobalt is given by,

$$\begin{aligned} V_i \frac{dQ_i}{dt} + \sum_{M=1}^{N_i} (f^M \hat{i} + g^M \hat{j} + h^M \hat{k}) \cdot \hat{n}^M \mathbf{d}^M \\ = \sum_{M=1}^{N_i} (r^M \hat{i} + s^M \hat{j} + t^M \hat{k}) \cdot \hat{n}^M \mathbf{d}^M \end{aligned} \quad (22)$$

where the subscript i and superscript M denote quantities for the i^{th} cell and the M^{th} face of cell i , respectively, and N_i is the number of faces bounding cell i .

Grid Information and Computational Approach:

Ahmed grid used in the present simulation is created by using Gridgen. An unstructured grid with 1,714,106 cells is used. Present case is run on the cluster of 256 parallel CPUs on blue horizon supercomputer at SDSC. Flow solution CPU time for DES is 6.4382 sec/iteration and for RANS is 6.3188 sec/iteration.

RESULTS AND DISCUSSION

Investigations of two different turbulence models, DES and RANS, have been carried out in the present study. Figure 3 to 6 shows the flow characteristics obtained by using DES model and Figure 7 thru 10 compare the DES and RANS results in terms of predicting C_d (coefficient of drag) and capturing flow details. The flow direction is in X direction and Z plane is the plane of symmetry.

Figure 3 shows the complex flowfield created during the wake flow of any ground vehicle. This particular flowfield is for the Ahmed Reference model with 25 degrees base slant angle. The salient point of the present simulation is the presence of the unsteady wake flow structure details. It is evident that there are several localized regions of counter rotating vortex formation. The existence of these circulatory regions suggests that large part of flow energy is present in various small pockets, namely vortices. The flow pattern shows the similarity with the flow described by Ahmed et al.² Though it is not exactly same, one can observe the presence of counter rotating vortices and separation bubble described by Ahmed et al.²

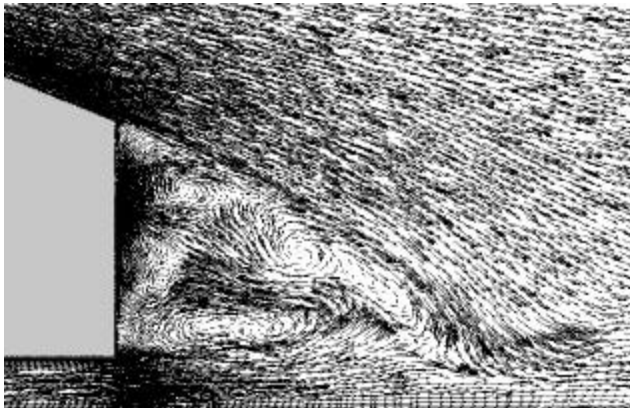


Figure 3. Wake flow structure at the plane $Z = 50\text{mm}$.

It also falls in the range of three-dimensional hatchback flow described by Gillieron and Chometon⁴ for the rear slant angles between upper and lower critical angles. They defined lower critical angle as 12° and upper critical angle as 30° . This simulation, though done for a short time duration (4.5 seconds), does reproduce the essential

features of the wake flow structure seen by Ahmed et al.² Generally, one can see that the large vortices are formed slightly away from the base region. It is anticipated that these counter rotating vortices, one below the other, towards the far end of the figure will peel off and merge.

Figure 4 shows the velocity vectors in yz plane. The counter rotating dipolar vortices are clearly seen from the figure. The symmetry of the circulation can be easily seen from the plotted vectors. The direction of rotation inside any of the dipolar vortex is opposite to each other at both the ends indicating positive and negative velocity regions. The dipolar structure displays a overall symmetry and together both the dipolar structure can be seen as forming a quadruple.

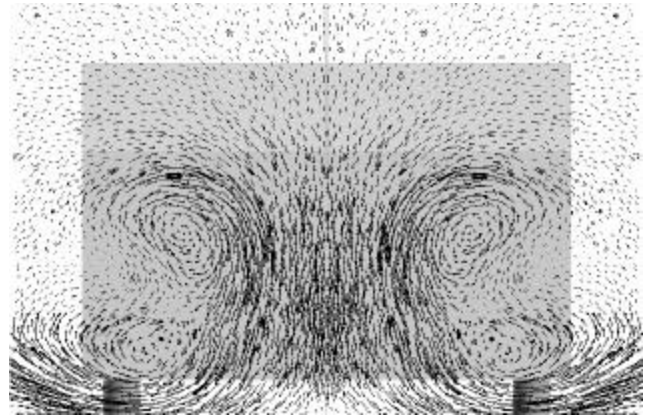


Figure 4. Velocity vectors in YZ plane at $X = 1100\text{mm}$.

Figure 5 shows the Mach number distribution at different regions close to the solid surface of the Ahmed reference model. The surface is cut along the Z-plane. Dark black color indicates low (0.03-0.05) value of Mach number and light gray color indicates high value of the same and the transition from dark black to light gray shows the increase in mach number. It is clearly seen that mach number is less near the frontal area of the vehicle and this happens due to the collision between the fluid and the solid surface. The value of mach number in this region falls in the range of 0.05 to 0.09. Further, maximum drop in the mach number is observed in the wake region. Dark black color indicates the lowest value of mach number, which is 0.03 and this drop is found in the area just behind the vehicle base. The length of this area of sudden drop along the flow direction is approximately 200mm. Flow separation and the presence of recirculation are two possible reasons for this drop. The highest mach number of 0.26 is observed near the side surface of the vehicle where the flow compression is responsible for this peak.

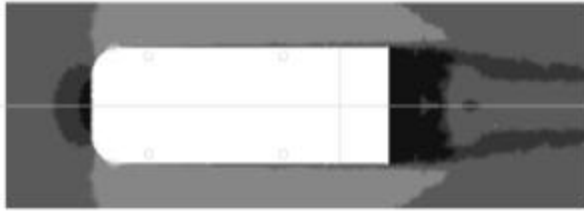


Figure 5. Mach number distribution at Y = 104 mm.

Figure 6 shows the pressure contours close to the base of the Ahmed model (X=1110mm). Dark black contours at the upper corners of the vehicle slant base shows low pressure region with the lowest value at the center of the circle (i.e. 100300pascal). Pressure plot indicates the presence of counter rotating vortices. The contour patterns observed here for pressure ranging from 100.3 kPa to 101.325 kPa is similar to the contours seen by Howard and Pourique¹² who used LES turbulence model. From figure 3 and figure 6 one can say that despite some striking similarities, in the present simulation, results show more complicated and unsteady nature of the wake flow than that of Gillieron and Chometon.⁴



Figure 6. Pressure contours at x=1111 mm.

From the iso-surface of the zero streamwise velocity, noticeable differences can be observed between the RANS (figure 7) and the DES (figure 8) solution. The three dimensional unsteady structure at the trailing edge of the DES solution is absent in time averaged RANS case. Clearly, DES is able to resolve the flow details better than the RANS mode for the same time-step. Figure demonstrates that DES is a better model if the details of the given flow structure is desired at a certain timestep. However, for gross features, RANS and DES are both reasonably appropriate.

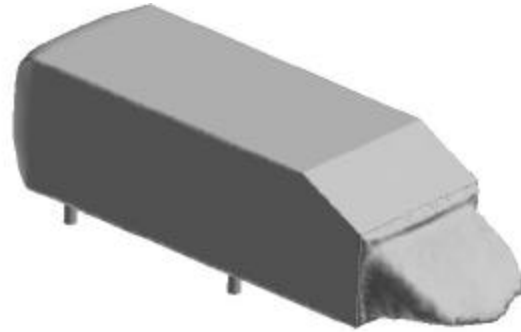


Figure 7. Iso-surface of zero streamwise velocity using Reynolds Averaged Navier Stokes.

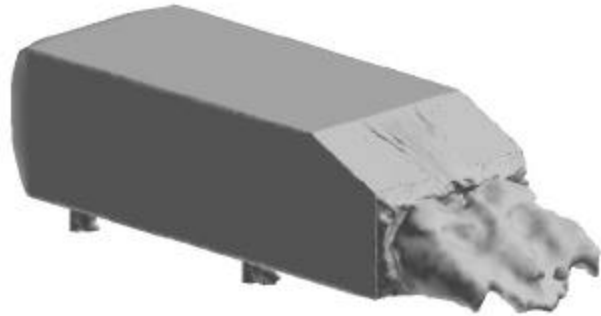


Figure 8. Iso-surface of zero streamwise velocity using detached eddy simulation.

Drag Calculation:

Following equation is used to calculate total drag coefficient (C_d) for both front and back part of the vehicle body.

$$C_d = \frac{F_d}{q A_{ref}} \quad (23)$$

$$q = \frac{1}{2} \rho u_\infty^2$$

where F_d is the total drag force acting on the body, which is the summation of the drag force at the front and back area of the vehicle, A_{ref} is the reference area, ρ is the fluid density and u_∞ is the freestream velocity. Two parameters, normal pressure and skin friction, are responsible for producing the drag. Ahmed et al.² described the effect of different base slant angles on C_d and contribution of each component (normal pressure and skin friction) in the total drag. He observed that pressure drag contributes 76% to 85% of the total drag and it also depends upon the rear slant angle as pressure drag increases with slant angle approaching the critical angle (30°).

Figures 9 and 10 show the unsteady nature of C_d and also the contribution of front and back in creating the total drag. In both figures, 'f' indicates front part of the vehicle body, 'b' indicates back part of the vehicle body and 't'

indicates total. Evidently, the back part of the body is a major contributor of the total drag. Large oscillations in the value of C_d can be observed during initial time-steps for both DES and RANS. After approximately 3 seconds, these oscillations become small and C_d approaches constant value. Similar characteristics can be found for the individual drag co-efficient of front and back part of the body. Average value of C_d in the case of DES is 0.2585 and in the case of RANS is 0.3272.

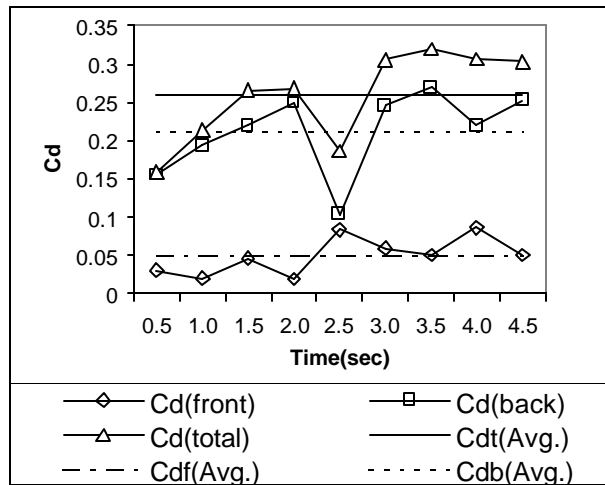


Figure 9. Time-study of C_d (DES)

The average value of C_d obtained by using DES is comparable with the result of Ahmed et al.² Though he did not calculate the value of C_d at 25°, from the interpolation of the value of C_d obtained by him for other angles, C_d falls in the range of 0.25 to 0.30 and is more towards 0.25. Thus, result obtained by using DES agrees with the experimental result of Ahmed et al.² Though RANS model exhibits some difference in the value of C_d from Ahmed et al.,² it shows similarity with the result obtained by Gillieron and Chometon⁴, which falls in the range between 0.33 and 0.35. This similarity can be related with the turbulence modeling technique used in both simulations. Present simulation uses S-A one equation RANS model while Ref 4 uses k-ε two-equation RANS model.

CONCLUSIONS

Wake flow simulation of Ahmed reference model with 25° rear slant angle is carried out in the present study by using DES as a turbulence model. Further, results are obtained by using RANS model for same time-steps and compared with DES results at a particular time-step. This comparison shows the ability of DES in capturing unsteady structure of the flow with minor flow details than RANS. Co-efficient of drag is calculated in both simulations and compared with established results. This

comparison finds similarity between DES results and experimental work by Ahmed et al.² and similarity between RANS results and numerical results of Gillieron and Chometon.⁴

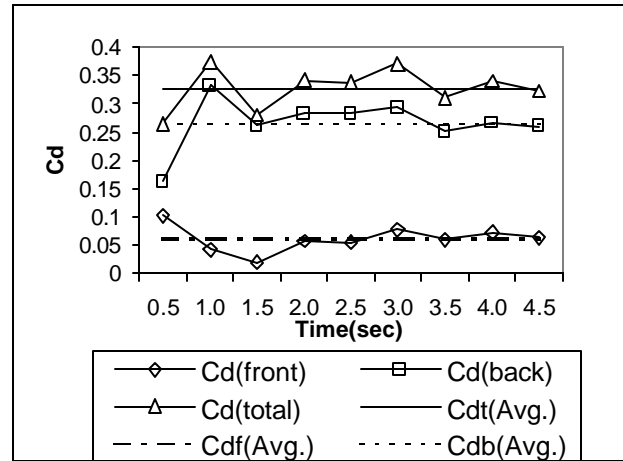


Figure 10. Time-Study of C_d (RANS).

References:

- Chometon, F. and Gillieron, P., "A Survey of Improved Techniques for Analysis of 3D Separated Flows in Automotive Aerodynamics", SAE Technical Paper Series 960 680, Feb 1996.
- Ahmed, S. R., Ramm, G. and Faltin, G., "Some Salient Features of the Time-Averaged Ground Vehicle Wake", SAE Technical Paper Series 840 300, Detroit 1984.
- Morel, T., "The effect of base slant angle on the flow pattern and drag of three-dimensional bodies with blunt ends", Proceedings of Symposium on Aerodynamic Drag Mechanisms of Bluff Bodies and Road Vehicles, Plenum Press, New York, 1978, pp.191-226.
- Gillieron, P. and Chometon, F., "Modelling of Stationary Three-Dimensional Separated Air Flows around an Ahmed Reference Model", ESAIM: Proceedings, Vol. 7, pp. 173-182, 1999.
- Strang, W. Z., Tomaro, R. F. and Grismer, M. J., "The Defining Methods of Cobalt₆₀ : A Parallel, Implicit, Unstructu Euler/Navier-Stokes Flow Solver", AIAA-99-16635, Jan 1999.
- Grismer, M. J., Strang, W. Z., Tomaro, R. F. and Witzeman, F. C., "Cobalt: A parallel, implicit, unstructured Euler/Navier-Stokes solver", Advances in Engineering Software, Vol. 29, No. 3-6, pp.365-373, 1998.

- ⁷Forsythe, J. R., Squires, K. D., Wurtzler, K. E. and Spalart, P. M., "Detached-Eddy Simulation of Fighter Aircraft at High Alpha", AIAA-02-0591, Jan 2002.
- ⁸Pope, S. B., "Turbulent Flows". Cambridge University Press, Cambridge, United Kingdom, 2000.
- ⁹Squires, K. D., Forsythe, J. R., Morton, S. A., Strang, W. Z., Wurtzler, K. E., Tomaro, R. F., Grismer, M. J. and Spalart, P. R., "Progress on Detached-Eddy Simulation of Massively Separated Flows", AIAA-02-1021, Jan 2002.
- ¹⁰Morton, S. A., Forsythe, J. R., Mitchell, A. M. and Hajek, D., "DES and RANS simulations of delta wing vortical flows", AIAA-02-0587, Jan 2002.
- ¹¹Han, T., "Computational Analysis of Three-Dimensional Turbulent Flow Around a Bluff Body in Ground Proximity", AIAA Journal, Vol. 27, No. 9, September 1989.
- ¹²Howard, R. J. A. and Pourquie, M., "Large eddy simulation of an Ahmed reference model", Journal Of Turbulence, Vol. 3, 2002, 012.
- ¹³Godunov, S. K., "A difference scheme for numerical computation of discontinuous solution of hydrodynamic equations", Journal Of Computational Physics, Vol. 32, pp.101-136, 1979.
- ¹⁴ Tannehill, J. C., Anderson, D. A. and Pletcher, R. H, "Computational Fluid Mechanics and Heat Transfer, Second Edition", Taylor & Francis, Philadelphia, 1997.
- ¹⁵Spalart, P. R., "Trends In Turbulence Treatment", AIAA-00-2306, June 2000.
- ¹⁶Strelets, M., "Detached Eddy Simulation of Massively Separated Flows", AIAA -01-0879, Jan 2001.
- ¹⁷Spalart, P. R. and Allmaras, S. R., "A One-Equation Turbulence Model for Aerodynamic Flows", AIAA-92-0439, Jan 1992.
- ¹⁸Spalart, P. R., Jou W-H., Strelets, M. and Allmaras, S. R., "Comments on the Feasibility of LES for Wings, and on a Hybrid RANS/LES Approach", Advances in DNS/LES, 1st AFOSR Int. Conf. on DNS/LES, Aug 4-8, 1997, Greyden Press, Columbus, Ohio.
- ¹⁹Tomaro, R. F., Strang, W. Z. and Sankar, L. N., "Implicit algorithm for solving time dependent flows on unstructured grids", AIAA-97-0333, Jan 1997.
- ²⁰"Cobalt: Quick Start Manual", Cobalt Solutions, LLC, Ohio, 2002.